

Finite-difference time-domain modeling of dispersive-material photonic bandgap structures

Richard W. Ziolkowski

Department of Electrical and Computer Engineering, The University of Arizona, 1230 East Speedway, Tucson, Arizona 85721-0104

Masahiro Tanaka

Department of Electrical and Computer Engineering, The University of Arizona, 1230 East Speedway, Tucson, Arizona 85721-0104, and Department of Information Science, Gifu University 1-1 Yanagido, Gifu City, Gifu 501-11, Japan

Received July 30, 1998; accepted October 20, 1998

Photonic bandgap (PBG) structures constructed from lossy, dispersive dielectric and metallic materials are characterized in terms of their reflection and transmission properties. Particular emphasis is given to PBG structures with defects. These PBG structures are modeled analytically with an *ABCD* matrix method for their single-frequency response. They also are modeled numerically with a finite-difference time-domain approach to determine their operating characteristics over a wide set of frequencies in a single simulation. It is shown that material dispersion can significantly alter the characteristics of a PBG structure's frequency response. Metallic PBG structures at optical frequencies thus exhibit bandgap characteristics significantly different from those of their nondispersive dielectric counterparts. It is shown that microcavities whose mirrors are constructed from dispersive-material PBG structures can be designed to outperform similar nondispersive-mirror microcavities. © 1999 Optical Society of America [S0740-3232(99)03303-7]

OCIS codes: 000.4430, 260.2030, 350.3950, 160.4670, 350.5500.

1. INTRODUCTION

The photonic bandgap (PBG) structure has become an important subject in the microwave regime for microwave circuit design^{1,2} and in the optics regime for nanostructure waveguides and microcavity laser mirrors and filters.³⁻⁹ For example, a vertical-cavity surface-emitting laser is basically a PBG structure with a defect.

One-dimensional (1D), multilayer PBG structures have been analyzed successfully by using an *ABCD* matrix formulation.¹⁰ This method has been used to reveal the salient features of a variety of dielectric PBG structures. Unfortunately, as the frequency of the optical wave becomes higher and higher, the refractive index of each layer cannot be considered to be constant with respect to frequency; i.e., the dispersive properties of the materials become significant. Although this may not be an issue for any single frequency, few integrated optics devices have the luxury of being designed without consideration of their behavior in multiwavelength applications.

In this paper we introduce dispersion properties into the PBG structures by incorporating a Lorentz material model for the polarization fields in the component materials. This allows us to study in detail the effects of dispersion on a variety of 1D PBG structures. In particular, we have determined these effects for PBG structures composed of both metallic and dielectric materials. Since metals at optical frequencies act as lossy, dispersive dielectrics,¹¹ they have been a natural candidate for our study. As will be demonstrated, dispersive effects significantly alter the optical operating characteristics of any

PBG structure. This is particularly true if the resonance frequency of the Lorentz model is near the center frequency of the band gap. As the resonance frequency moves toward that center frequency, out-of-band properties of the PBG migrate toward the bandgap and distort the band structure. Bandgaps and passbands appear in unanticipated regions. Moreover, the individual bandgaps widen as the dispersive effects become stronger. The metal/dielectric bandgap structures, despite the presence of metals with very shallow skin depths, can be designed to have strong transmissive properties that could be used for interesting filtering applications. This effect has actually been demonstrated experimentally in Ref. 12. Having determined their reflection and transmission properties, we then incorporated defects into these PBG structures to form microcavities. The results of our investigation demonstrate that microcavities whose mirrors are constructed from dispersive PBG structures can be designed to have operating characteristics at particular frequencies that are superior to those of similar nondispersive-mirror microcavities.

We not only investigated this dispersive material PBG structure with an appropriate extension of the standard *ABCD* matrix approach but also introduced a finite-difference time-domain (FDTD) full-wave, vector Maxwell approach, combined with the fast Fourier transform (FFT) method, to analyze these structures. Simulations with the two approaches are shown to yield the same results. This 1D investigation thus allows us to use the analogous FDTD approach with confidence in our two-

and three-dimensional PBG studies, which are currently in progress. The FDTD approach allows one to obtain the frequency response of finite PBG structures over a wide set of frequencies in a single simulation as well as a complete visualization of the time evolution of all the associated field and material quantities. Since we are also currently studying nanostructure waveguides formed from defects in finite-sized PBG's, the FDTD approach permits us to investigate the temporal evolution of the propagation of the associated electromagnetic guided waves.

2. FINITE-DIFFERENCE TIME-DOMAIN SIMULATOR

We assume that the PBG structure varies only along the z axis and is uniform on any x - y plane. Thus all the electromagnetic waves are planar, with the electric and magnetic fields being constant in any x - y plane and the direction of propagation being along the z axis. We take these plane waves to be x polarized (electric field along the x axis and magnetic field along the y axis) throughout.

A. Lorentz Model

To include dispersion in the materials, we introduce the Lorentz model for the polarization field \mathbf{P} . Since the electric field has the form $\mathbf{E} = E_x \hat{x}$, the polarization field has the form $\mathbf{P} = P_x \hat{x}$ and satisfies the equation

$$\frac{\partial^2 P_x}{\partial t^2} + \Gamma \frac{\partial P_x}{\partial t} + \omega_0^2 P_x = \epsilon_0 \omega_p^2 \chi_L E_x, \quad (1)$$

where Γ is the damping coefficient, ω_0 is the resonance frequency, ω_p is the plasma frequency, and χ_L is related to the dc value of the electric susceptibility χ_{dc} as $\chi_{dc} = (\omega_p^2 \chi_L) / \omega_0^2$. The associated frequency domain expression

$$P_{x,\omega} = \frac{\epsilon_0 \omega_p^2 \chi_L}{\omega_0^2 - \omega^2 + j\omega\Gamma} E_{x,\omega} \quad (2)$$

is obtained by Fourier transform of Eq. (1). Figure 1 indicates the relation between the frequency and the refractive index $n(\omega) = [1 + \chi(\omega)]^{1/2}$, where the frequency-domain susceptibility $\chi(\omega) = P_{x,\omega} / \epsilon_0 E_{x,\omega}$ when $\omega_0 = \omega_p = \omega_C$, $\Gamma = 0.01\omega_C$ and $\chi_L = 1$ and where ω_C acts as a

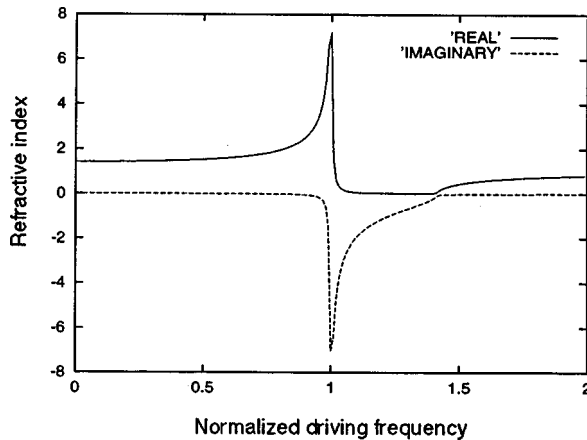


Fig. 1. Refractive index versus normalized driving frequency in the case in which $\omega_0 = \omega_p = \omega_C$, $\Gamma = 0.01\omega_C$ and $\chi_L = 1$.

reference frequency and will be called the center frequency. These values will be assumed throughout all of the numerical calculations unless otherwise indicated. Referring to Fig. 1, one finds essentially four regions of interest: (1) The real part of the index is increasing only with the frequency; (2) the real and imaginary parts of the index are very large (near resonance); (3) the real part of the index is nearly zero and the imaginary part is large; and (4) the real part of the index is increasing but is less than one and the imaginary part is nearly zero.

If $\omega_0 \gg \omega$, then the polarization field takes a simple form: $P_{x,\omega} = (\epsilon_0 \omega_p^2 \chi_L / \omega_0^2) E_{x,\omega}$. In this dipole approximation, $P_{x,\omega} = \epsilon_0 \omega_{dc} E_{x,\omega}$ and the electrical susceptibility is constant, so the refractive index is $n_{dc} = (1 + \chi_{dc})^{1/2}$. On the other hand, as the frequency approaches infinity, clearly the electrical susceptibility goes to zero. Our interest is mainly in the frequency region $\omega \geq \omega_C$, where these approximations are invalid and the full model must be used.

B. Finite-Difference Time-Domain Formulation

In the FDTD approach the simulation space (region of interest) is discretized into cells of length Δz , and time is discretized into intervals of length Δt . Using the standard leapfrog in time and the staggered-grid approach, the electric field is taken at the edge of a cell and at integer time steps so that $E_x(z, t) = E_x(k\Delta z, n\Delta t)$ is represented by $E_x^n(k)$, and the magnetic field is taken at the center of the cell at half-integer time steps so that $H_y(z, t) = H_y[(k + 1/2)\Delta z, (n + 1/2)\Delta t]$ is represented by $H_y^{n+1/2}(k + 1/2)$. The FDTD formulation for the propagation of 1D electromagnetic waves in the PBG structure is then obtained directly from Maxwell's equations and can be expressed as follows:

$$H_y^{n+1/2}\left(k + \frac{1}{2}\right) = H_y^{n-1/2}\left(k + \frac{1}{2}\right) - \frac{\Delta t}{\mu_0} \frac{E_x^n(k+1) - E_x^n(k)}{\Delta z}, \quad (3)$$

$$E_x^{n+1}(k) = E_x^n(k) - \frac{\Delta t}{\epsilon_0} \times \left[\frac{H_y^{n+1/2}(k+1/2) - H_y^{n+1/2}(k-1/2)}{\Delta z} + J_x^{n+1/2}(k) \right]. \quad (4)$$

The Lorentz model [Eq. (1)] is incorporated self-consistently¹¹ into Maxwell's equations by introducing the equivalent first-order system through the definition of the polarization current; i.e.,

$$J_x = \frac{\partial P_x}{\partial t}, \quad (5)$$

$$\frac{\partial J_x}{\partial t} + \Gamma J_x = \epsilon_0 \omega_p^2 \chi_L E_x - \omega_0^2 P_x. \quad (6)$$

The electric current and the polarization field are taken at the same spatial location as the electric field, but the electric current is taken at the same time value as the magnetic field while the polarization field is taken at the same time value as the electric field; i.e., $J_x(z, t)$ and $P_x(z, t)$ are represented, respectively, by $J_x^{n+1/2}(k)$ and

$P_x^n(k)$. Discretizing Eqs. (5) and (6) with finite differences yields the desired updated equations:

$$J_x^{n+1/2}(k) = \left(\frac{1 - \frac{\Gamma\Delta t}{2}}{1 + \frac{\Gamma\Delta t}{2}} \right) J_x^{n+1/2}(k) + \left(\frac{\Delta t}{1 + \frac{\Gamma\Delta t}{2}} \right) \times [\epsilon_0 \omega_p^2 \chi_L E_x^n(k) - \omega_0^2 P_x^n(k)], \quad (7)$$

$$P_x^{n+1}(k) = P_x^n(k) + \Delta t J_x^{n+1/2}(k). \quad (8)$$

The resulting system of equations [Eqs. (3), (4), (7), and (8)] is solved at each time step for all of the field and current values. One thus obtains the full time evolution of the system. To obtain the corresponding frequency-domain information, one must apply a FFT to the resulting time signals. One can study the behavior of the PBG structure over a wide bandwidth by simply exciting it with an ultrafast pulse that has a wide spectral content. The resulting fields will contain the desired frequency-domain information, e.g., the reflection and transmission coefficients as functions of the frequency.

The FDTD simulator is used to obtain the reflection and transmission coefficients at a wide band of frequencies in one run. The PBG structure is excited with a single-cycle pulse whose bandwidth encompasses the frequency region of interest. This input signal is launched from a total field/scattered field interface^{11,13}; it is measured on this interface. The reflected field is measured in time at a point in the scattered field region behind the source; the transmitted field is measured in time at a point beyond the PBG structure. The resulting fields are transformed with a FFT to produce their frequency spectra. The reflected and transmitted field spectra are then divided by the input signal spectrum to generate the reflection and transmission coefficients.

3. LOSSLESS DIELECTRIC ONE-DIMENSIONAL PHOTONIC BANDGAP STRUCTURES

The 1D PBG structure without a defect that will be discussed below is shown as Fig. 2(a). It is composed of N pair of layers of medium 1 and medium 2 and an extra layer of medium 1, where the plane-wave source is taken outside the PBG structure. Thus the total number of layers in this structure is $n = 2N + 1$. The locations in z of each interface are labeled as indicated. This choice of layers makes the structure symmetric about its center.

The analytic formulas for the reflection and transmission coefficients of a 1D PBG layered structure reduce to simple expressions when the width of each layer is a quarter of the driving wavelength in that material. In particular, the reflection and transmission coefficients for the 1D PBG in Fig. 2(a) are readily obtained with the $ABCD$ matrix approach¹⁰ in general; and when the length of each region is a quarter wavelength in that material, the coefficients can be expressed as

$$R = \frac{(\epsilon_2/\epsilon_1)^N(\epsilon_0/\epsilon_1) - 1}{(\epsilon_2/\epsilon_1)^N(\epsilon_0/\epsilon_1) + 1} \exp(j2k_0d_0), \quad (9)$$

$$T = 2j(-1)^N \frac{(\epsilon_2/\epsilon_1)^{N/2}(\epsilon_0/\epsilon_1)^{1/2}}{(\epsilon_2/\epsilon_1)^N(\epsilon_0/\epsilon_1) + 1} \times \exp[jk_0(d_{2N+1} - d_0)]. \quad (10)$$

The 1D PBG structure with a defect that will be discussed below is shown as Fig. 2(b). It is composed of M pairs of layers of medium 1 and medium 2, an extra layer of medium 1 (i.e., $m = 2M + 1$ total layers), the defect layer, N pairs of layers of medium 1 and medium 2, and an extra layer of medium 1 (i.e., $n = 2N + 1$ total layers). Thus the total structure consists of $m + 1 + n$ layers. When $N = M$, the resulting microcavity is symmetric about the defect; we will refer to it as an n -layer-mirror microcavity. The reflection and transmission coefficients for the general 1D PBG defect structure are also readily obtained with the $ABCD$ matrix approach and in the quarter-wavelength special case can be expressed as

$$R = \frac{(\epsilon_2/\epsilon_1)^{M+N}[(\epsilon_0\epsilon_{def})/\epsilon_1^2] - 1}{(\epsilon_2/\epsilon_1)^{M+N}[(\epsilon_0\epsilon_{def})/\epsilon_1^2] + 1} \exp(j2k_0d_0), \quad (11)$$

$$T = 2j(-1)^{M+N+1} \frac{(\epsilon_2/\epsilon_1)^{(M+N)/2}[(\epsilon_0\epsilon_{def})/\epsilon_1^2]^{1/2}}{(\epsilon_2/\epsilon_1)^{M+N}[(\epsilon_0\epsilon_{def})/\epsilon_1^2] + 1} \times \exp[jk_0(d_{2M+2+2N+1} - d_0)], \quad (12)$$

these formulas are, of course, valid for only one particular operating frequency.

To check the FDTD simulator and the corresponding spectral-domain response-function procedure, we compared the results obtained with this approach with those generated by the $ABCD$ matrix method. Figures 3(a) and

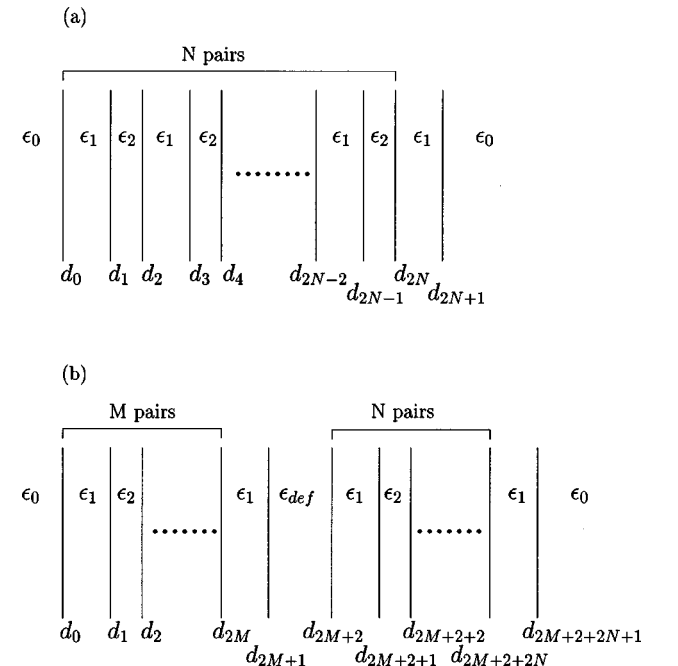


Fig. 2. PBG structures (a) without defect and (b) with defect.

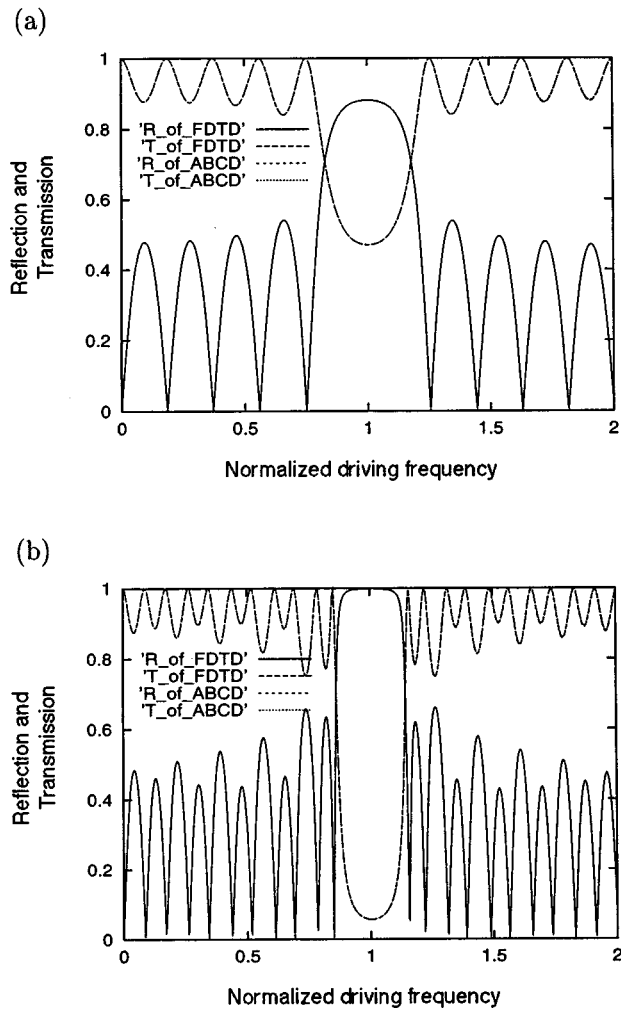


Fig. 3. Reflection and transmission coefficients versus normalized driving frequency for an 11-layer structure (a) without defect and (b) for a microcavity consisting of a defect layer sandwiched between a pair of 11-layer structures. The parameters of medium 1 are $\omega_{01} = 100\omega_C$, $\Gamma_1 = 0.01\omega_{01}$ and $\chi_{L1} = 1$. The parameters of medium 2 are $\omega_{02} = 100\omega_C$, $\Gamma_2 = 0.01\omega_{02}$, and $\chi_{L2} = 3$.

Table 1. FDTD Dispersion-Model Parameters

	Damping Coefficient	Electric Susceptibility
Medium 1	$\Gamma_1 = 0.01\omega_{01}$	$\chi_{L1} = 1$
Medium 2	$\Gamma_2 = 0.01\omega_{02}$	$\chi_{L2} = 3$
Defect	$\Gamma_d = 0.01\omega_{0d}$	$\chi_{Ld} = 4$

3(b) show the reflection and transmission coefficients associated with an 11-layer structure [$N = 5$ in Fig. 2(a)] and an 11-layer-defect-11-layer structure [$M = N = 5$ in Fig. 2(b)]. The FDTD simulator includes the dispersive media in each region; these materials are run with the parameters shown in Table 1. These Lorentz dispersion-model parameters are used throughout this paper. The resonance frequencies in this case are assigned the same values in media 1 and 2 and in the defect to achieve frequency-independent media values for com-

parison with the $ABCD$ matrix results. These resonance-frequency values are $\omega_{01} = \omega_{02} = \omega_{0d} = 100\omega_C$, where the center frequency ω_C is 2.417×10^{15} (wavelength $\lambda_C = 780$ nm). With these choices the media are effectively nondispersive, and the refractive indices of media 1 and 2 and the defect are, respectively, $\sqrt{2}$, 2, and $\sqrt{5}$.

For the FDTD calculations the space and time discretizations were taken to be $\Delta z = \lambda_C/1000$ and $\Delta t = \Delta z/2c$, where $c = 3 \times 10^8$ m/s is the speed of light. These discretizations are very small so that we can model very accurately the response of the PBG structure in both the nondispersive- and the dispersive-media cases. These choices for the space and time discretizations are assumed throughout this paper.

As Figs. 3(a) and 3(b) demonstrate, the reflection and transmission coefficients obtained with the FDTD simulator and with the analytical $ABCD$ matrix multiplication approach were identical for the PBG structure without and with the defect. These results and those obtained for several other related configurations validated the FDTD simulator and the associated FFT postprocessing approach.

4. DISPERSIVE DIELECTRIC ONE-DIMENSIONAL PHOTONIC BANDGAP STRUCTURES

Having validated our approach on dispersionless PBG structures, we then used the FDTD simulator to model dispersive PBG configurations with and without defects. Several structures were considered and are described below. We also extended the $ABCD$ matrix approach to dispersive materials to provide validation cases. For all of the PBG structures the effects of dispersion on the reflection and transmission coefficients were obtained. The results from the $ABCD$ matrix and the FDTD approaches agreed in all cases.

A. Dispersive Photonic Bandgap Structures without Defects

We first investigated cases in which either medium 1 or medium 2 was dispersive and the other was nondispersive. Results for the reflection and transmission coefficients of a simple version of the structure shown in Fig. 2(a), i.e., one with $N = 1$ (three-layer structure), are given in Fig. 4. The resonance frequency in medium 1 was fixed at $100\omega_C$, and in medium 2 it was varied among the values $100\omega_C$, $3\omega_C$, $2\omega_C$, ω_C , and $0.5\omega_C$. The damping coefficients and the electric susceptibilities of both medium 1 and medium 2 were the same as those given in Table 1. Consequently, medium 1 was a nondispersive material whose index was $\sqrt{2}$, and medium 2 was dispersive with a low-frequency index of 2.

Figures 4(a) and 4(b) show that the character of the reflection and transmission coefficients is significantly different from that of the nondispersive case. The locations of the peaks and valleys has shifted, and the symmetry of the curves with respect to the center frequency of the exciting pulse is completely lost. In particular, as ω_{02} is decreased, these reflection and transmission coefficient curves exhibit more resonancelike behaviors and their

peaks shift to lower frequencies. We explain these results by using the following analytical formulas.

The reflection coefficient for this structure can be deduced analytically with the *ABCD* matrix method and is expressed as

$$R_{01} = \frac{n_0 - n_1}{n_0 + n_1}, \tag{16}$$

$$R_{12} = \frac{n_1 - n_2(\omega_C)}{n_1 + n_2(\omega_C)}, \tag{17}$$

$$R = \exp(-j2k_0d_0) \frac{f(\omega) - g(\omega)\exp\left[-j\pi\frac{n_2(\omega)\omega}{n'_2\omega_C}\right]}{\left[1 + R_{01}R_{12}\exp\left(-j\pi\frac{\omega}{\omega_C}\right)\right]^2 - \left[R_{01}\exp\left(-j\pi\frac{\omega}{\omega_C}\right) + R_{12}\right]\exp\left[-j\pi\frac{n_2(\omega)\omega}{n'_2\omega_C}\right]}, \tag{13}$$

where

$$f(\omega) = R_{01} + R_{12}(1 + R_{01}^2)\exp[-j\pi(\omega/\omega_C)] + R_{01}R_{12}^2\exp[-j2\pi(\omega/\omega_C)], \tag{14}$$

$$g(\omega) = R_{01}R_{12}^2 + R_{12}(1 + R_{01}^2)\exp[-j\pi(\omega/\omega_C)] + R_{01}\exp[-j2\pi(\omega/\omega_C)], \tag{15}$$

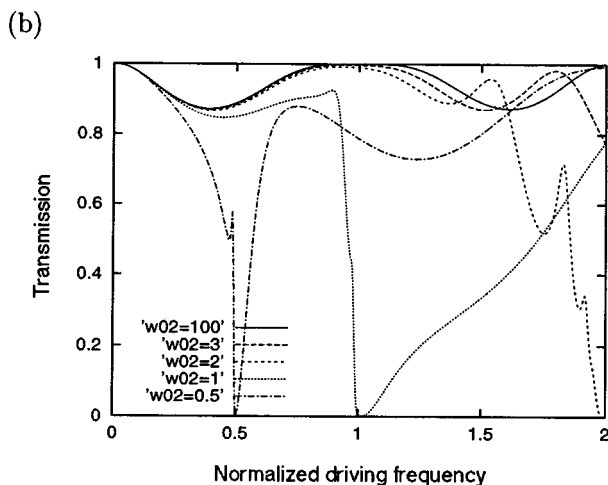
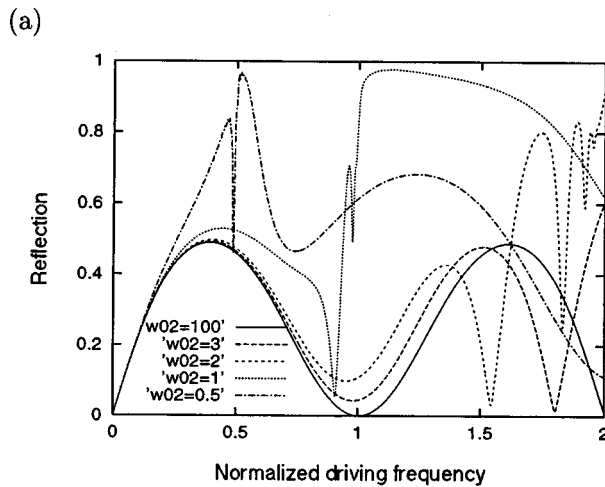


Fig. 4. (a) Reflection and (b) transmission coefficient versus normalized driving frequency for a three-layer structure. The parameters of media 1 and 2 are $\omega_{01} = 100\omega_C$ and $\omega_{02} = 100\omega_C, 3\omega_C, 2\omega_C, \omega_C,$ and $0.5\omega_C$.

and where n_0 and n_1 represent the refractive indices in free space and in medium 1, while $n_2(\omega)$ and n'_2 denote the dispersive index and the dc index in medium 2. If $n_2(\omega)$ is slightly larger than n'_2 , then one finds that the frequency point at which the term $\exp\{-j\pi[n_2(\omega)\omega]/(n'_2\omega_C)\}$ has the same value as the term $\exp[-j\pi(\omega/\omega_C)]$ (in the nondispersive-material case) shifts to lower frequencies as the center frequency is decreased. This explains why the peaks and valleys of the curves in Figs. 4(a) and 4(b) shift to lower frequencies with decreasing ω_{02} .

Since the index $n_2(\omega)$ varies as a polynomial function of ω , it differs more from its dc value n'_2 with increasing frequency. The variations of the reflection and transmission coefficients increase correspondingly even at frequencies with values much smaller than ω_{02} . This is clear in the cases with $\omega_{02} \leq 2\omega_C$. However, there is little effect on the cases with $\omega_{02} > 2\omega_C$ because the term $n_2(\omega)/n'_2$ is not large enough in comparison with the ratio ω/ω_C to make the phase term $\exp\{-j\pi[n_2(\omega)\omega]/(n'_2\omega_C)\}$ vary quickly enough.

We note that the reflection coefficient is nearly one and the transmission coefficient is nearly zero at the frequency $\omega \approx \omega_{02}$. Since the real and imaginary parts of the index are very large there, the term $\exp\{-j\pi[n_2(\omega)\omega]/(n'_2\omega_C)\}$ in Eq. (13) becomes very small in this region. Consequently, Eq. (13) becomes approximately

$$R \approx \exp(-j2k_0d_0) \frac{f(\omega)}{\{1 + R_{01}R_{12}\exp[-j\pi(\omega/\omega_C)]\}^2} \tag{18}$$

and $R_{12} \approx -1$, which shows that the dispersive-medium PBG structure can act as a medium with very high reflectivity. Correspondingly, the transmission coefficient is zero at a frequency slightly higher than ω_{02} , because medium 2 exhibits high loss and hence high reflectivity there. One can consider cases for which the reflection coefficient is near one and the transmission coefficient is near zero at frequencies slightly higher than ω_{02} even if $\omega_{02} = 100\omega_C$. This region clearly shifts to lower frequencies with decreasing ω_{02} , and the amount of variation in these coefficients increases.

Figures 5(a) and 5(b) show the reflection and transmission coefficients obtained for the corresponding cases in which the nondispersive and the dispersive layers are interchanged, i.e., the cases for which medium 1 is disper-

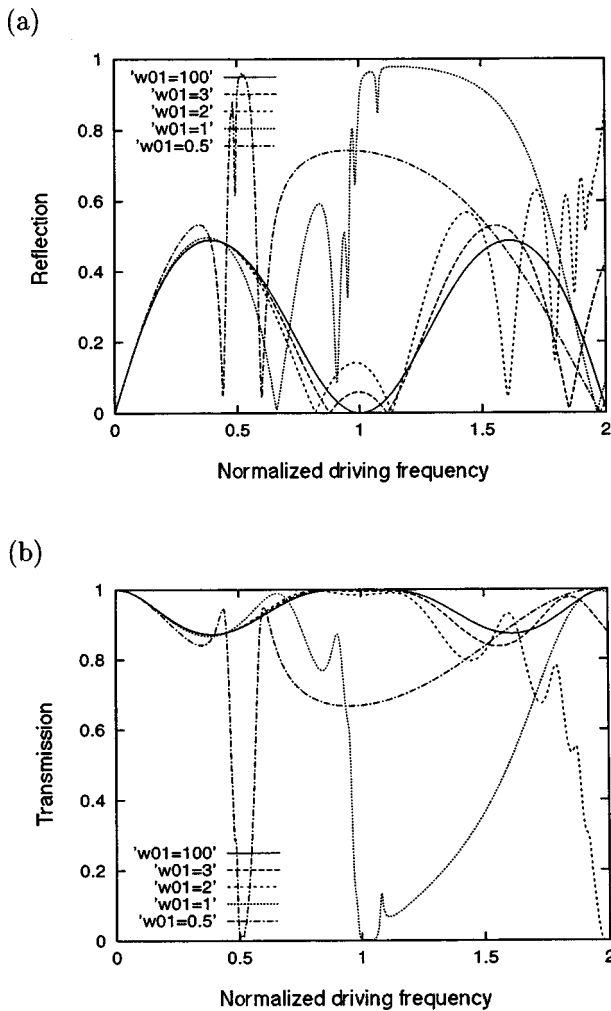


Fig. 5. (a) Reflection and (b) transmission coefficient versus normalized driving frequency for a three-layer structure. The parameters of media 1 and 2 are $\omega_{01} = 100\omega_C, 3\omega_C, 2\omega_C, \omega_C,$ and $0.5\omega_C,$ and $\omega_{02} = 100\omega_C.$

sive with its resonance frequency taking the values $\omega_{01} = 100\omega_C, 3\omega_C, 2\omega_C, \omega_C,$ and $0.5\omega_C$ and for which medium 2 is nondispersive with $\omega_{02} = 100\omega_C$ so that its refractive index is fixed at 2.

The basic characteristics of the reflection and transmission coefficients of these PBG structures are almost the same as they were in the previous cases. The differences become more pronounced as the differences in the variations away from the dc refractive indices increase. For one, more peaks appear in the reflection coefficient near the center frequency for the $\omega_{02} = 3\omega_C$ and $2\omega_C$ cases. For another, the transmission curve has a small peak that occurs between the frequencies ω_C and $1.1\omega_C$ in the case for which $\omega_{02} = \omega_C.$

Next we studied the dependence of the reflection and transmission properties of these basic PBG structures as a function of the number of layers. The results are summarized in Figs. 6(a) and 6(b); they represent the case for which the characteristic frequencies in media 1 and 2 are fixed at $\omega_{01} = 100\omega_C$ and $\omega_{02} = \omega_C,$ respectively. The curves show that in the lower-frequency region, the response of the PBG structure is highly dependent on the number of layers. Since the index varies little from its dc

value in this region, these results are expected from the nondispersive results. However, the behaviors are almost the same in the high-frequency regions as the number of layers is increased. These differences result from the fact that there are more dispersive layers as the total number of pairs is increased. There is only one dispersive layer in the three-layer structure. This is the reason that the curves for the three-layer structure do not correspond well with those for the five-and-more-layer structures. This was confirmed by exchanging the nondispersive and the dispersive layers. Figures 7(a) and 7(b), which show the reflection and transmission coefficients for the cases in which the nondispersive and the dispersive materials are exchanged, illustrate this effect. The resonance-frequency values in media 1 and 2 are $\omega_{01} = \omega_C$ and $\omega_{02} = 100\omega_C,$ respectively. The number of dispersive layers is now two for the three-layer structure. The curves of this three-layer structure, especially the reflection-coefficient one, are now more similar to the other structures. However, notice the disappearance of the bandpass structure near 1.3 for all of these structures. A large bandgap region forms at frequencies

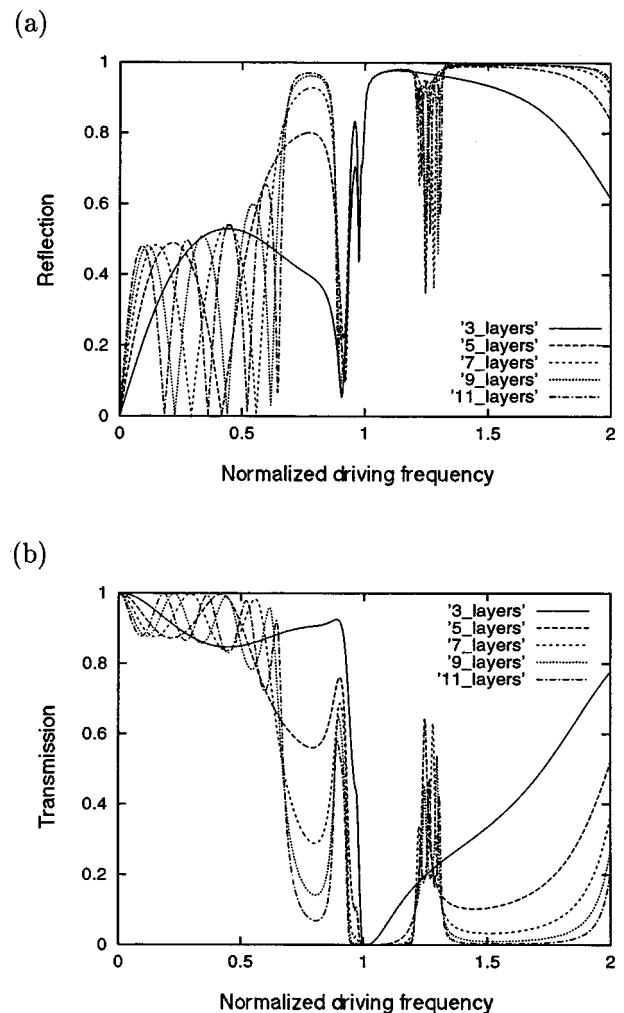


Fig. 6. (a) Reflection and (b) transmission coefficient versus normalized driving frequency for 3-, 5-, 7-, 9-, and 11-layer structures. The parameters of media 1 and 2 are $\omega_{01} = 100\omega_C$ and $\omega_{02} = \omega_C.$

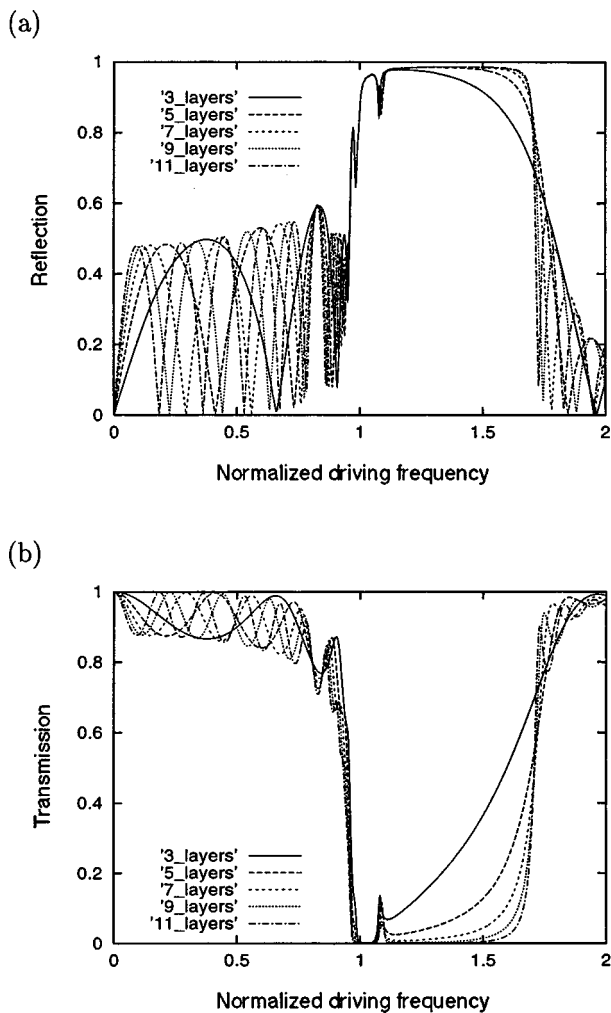


Fig. 7. (a) Reflection and (b) transmission coefficient versus normalized driving frequency for 3-, 5-, 7-, 9-, and 11-layer structures. The parameters of media 1 and 2 are $\omega_{01} = \omega_C$ and $\omega_{02} = 100\omega_C$.

above ω_C ; its edges become more pronounced as the number of layers increases. These comparisons clearly indicate that there are distinguishable effects in the response of PBG structures with two or more dispersive layers.

B. Dispersive Photonic Bandgap Structures with Air Defects

Having treated the basic PBG dispersive-material structure that is illuminated externally, we next consider the use of such structures as mirrors in source-driven microcavities. Results are given for dispersive-material PBG structures that have a quarter-wavelength air defect with a current (plane-wave) source located at the center of the defect. Thus the PBG structure forms a cavity about this source; the resulting transmitted fields should show enhancements as a result of the feedback caused by the reflections from the PBG mirrors that surround the source.

The first configuration modeled with the FDTD simulator was constructed from two three-layer PBG structures and the air defect. This case corresponds to the $M = 1$, $N = 1$ version of Fig. 2(b), i.e., a three-layer-mirror microcavity. The resonance frequency in medium 1 was fixed to be $\omega_{01} = 100\omega_C$, and its value in medium 2 was

varied among the values $\omega_{02} = 100\omega_C$, $3\omega_C$, $2\omega_C$, ω_C , and $0.5\omega_C$. Thus the cavity walls are dispersive and behave optically as discussed above. The defect medium was air but was modeled with the Lorentz model with $\chi_L = 0$.

The transmission-coefficient results for this microcavity structure are summarized in Fig. 8. Because of the properties of the three-layer-structure mirror shown in Figs. 4(a) and 4(b), it was expected that the peaks of the transmission coefficient would shift to the lower-frequency region as ω_{02} was decreased. The curves in Fig. 8 confirm this behavior. The interesting aspect of these shifts is that a cavity composed of dispersive-material walls—for instance, when $\omega_{02} = \omega_C$ and $\omega_{02} = 0.5\omega_C$ —can cause much higher transmission-coefficient values at particular frequencies than those generated with nondispersive mirrors. This is a result of the enhanced reflectivity of the PBG structure at those frequencies when the dispersive materials are present.

The effects of changing the amount of dispersion in the mirrors are readily ascertained by interchanging the dispersive and the nondispersive materials. Figure 9 shows the FDTD-predicted results for this case. The resonance frequency in medium 1 was now varied among the values $\omega_{01} = 100\omega_C$, $3\omega_C$, $2\omega_C$, ω_C , and $0.5\omega_C$, while its value in medium 2 was fixed to the value $\omega_{02} = 100\omega_C$. The basic character of the transmission-coefficient curve is similar to that of the preceding case except that the locations of the peaks are significantly altered. This is due to the differences in the reflectivity of the mirrors in this microcavity. We thus realize that the peaks are dependent on the material parameters and their relative distributions, as we can easily see by comparing Figs. 8 and 9. Without numerical analyses it would be extremely difficult to predict where the enhanced transmission coefficients would appear.

As was realized from the reflection and transmission studies, the microcavity behavior could be made much more distinct by increasing the number of layers. Figures 10 and 11 show the results for the cases in which the number of layers in the PBG microcavity walls varied from 3 to 11. The widths of the enhancement peaks and

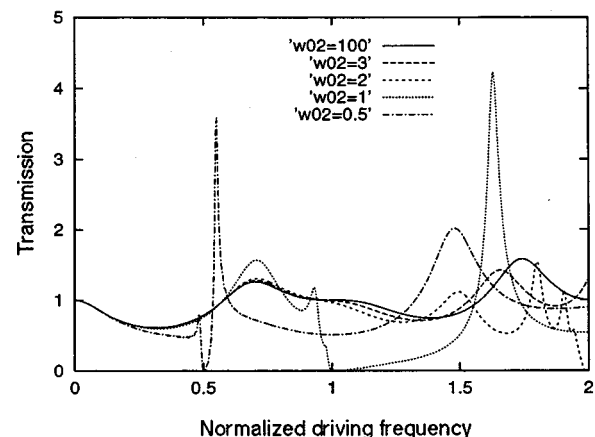


Fig. 8. Transmission coefficient versus normalized driving frequency for a three-layer-mirror PBG microcavity with an air defect. The parameters of media 1 and 2 are $\omega_{01} = 100\omega_C$ and $\omega_{02} = 100\omega_C$, $3\omega_C$, $2\omega_C$, ω_C , and $0.5\omega_C$.

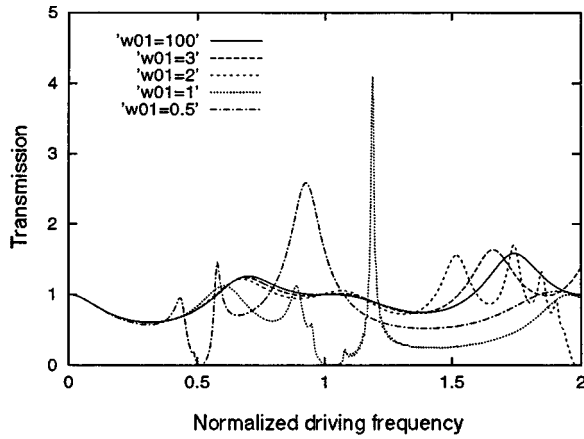


Fig. 9. Transmission coefficient versus normalized driving frequency for a three-layer-mirror PBG microcavity with an air defect. The parameters of media 1 and 2 are $\omega_{01} = 100\omega_C$, $3\omega_C$, $2\omega_C$, ω_C , and $0.5\omega_C$ and $\omega_{02} = 100\omega_C$.

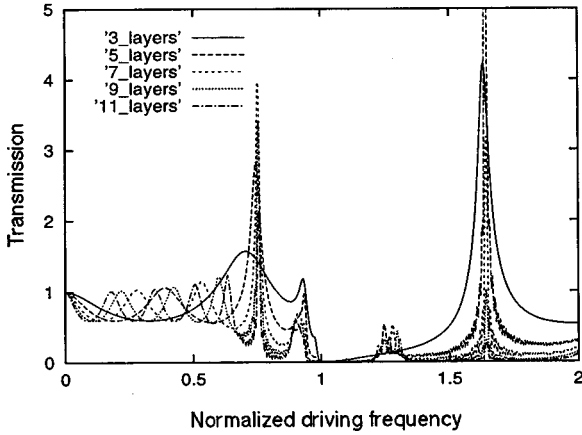


Fig. 10. Transmission coefficient versus normalized driving frequency for an n -layer-mirror PBG microcavity with an air defect. The parameters of media 1 and 2 are $\omega_{01} = 100\omega_C$ and $\omega_{02} = \omega_C$.

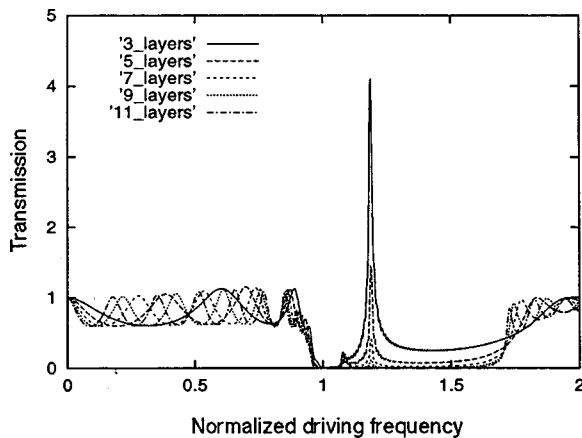


Fig. 11. Transmission coefficient versus normalized driving frequency for an n -layer-mirror PBG microcavity with an air defect. The parameters of media 1 and 2 are $\omega_{01} = \omega_C$ and $\omega_{02} = 100\omega_C$.

the maximum values of the peaks decrease with an increasing number of layers. As more layers are added, there is more loss, which decreases the peak values, and

there is a higher-cavity Q , which decreases the widths. Nonetheless, there are regions where the enhancement peaks remain significant. Moreover, the transmission coefficients become significantly smaller in the neighborhoods of the enhancement-frequency values. This means that one could design a dispersive microcavity structure to produce a much larger output at a specified frequency with a higher degree of isolation from neighboring frequencies than one could with nondispersive materials in the cavity walls.

C. Nondispersive Photonic Bandgap Structures with Dispersive Defects

To complete our study, we examined the reciprocal case for which the three-layer-mirror PBG microcavity is formed from nondispersive layers and a dispersive defect. The resonance frequency in media 1 and 2 was fixed at the values $\omega_{01} = \omega_{02} = 100\omega_C$, and in the defect region it was varied among the values $\omega_{0d} = 100\omega_C$, $3\omega_C$, $2\omega_C$,

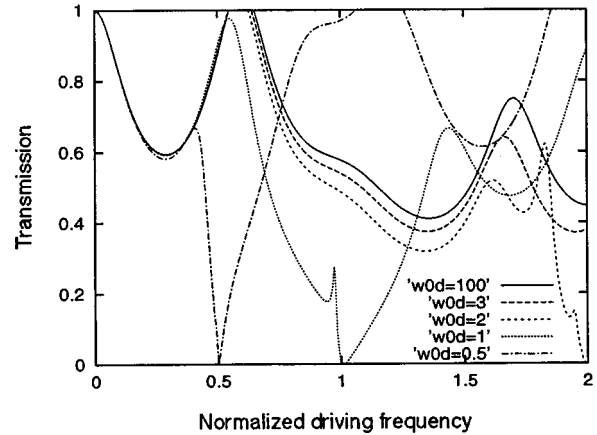


Fig. 12. Transmission coefficient versus normalized driving frequency for a nondispersive three-layer-mirror PBG microcavity with a dispersive defect. The parameters of media 1 and 2 are $\omega_{01} = 100\omega_C$ and $\omega_{02} = 100\omega_C$; for the defect region they are $\omega_{0d} = 100\omega_C$, $3\omega_C$, $2\omega_C$, ω_C , and $0.5\omega_C$.

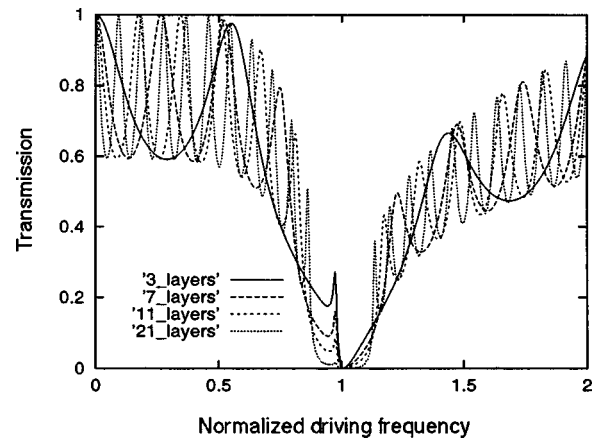


Fig. 13. Transmission coefficient versus normalized driving frequency in the case of an n -layer, nondispersive-mirror-microcavity PBG structure with a dispersive defect. The mirrors are composed of 3, 7, 11, and 21 layers. The parameters of media 1 and 2 are $\omega_{01} = 100\omega_C$ and $\omega_{02} = 100\omega_C$; for the defect region they are $\omega_{0d} = \omega_C$.

ω_C , and $0.5\omega_C$. The transmission properties of this microcavity are summarized in Fig. 12. This structure is found to perform poorly in comparison with the dispersive PBG structure with an air defect.

Figure 13 shows the transmission-coefficient results for the cases in which the number of layers in the nondispersive mirrors is increased when the resonance frequency in the defect is fixed at $\omega_{0d} = \omega_C$. The curves clearly become more complicated with an increasing number of layers, but their basic character does not change. This is a reasonable result since the properties of the dispersive defect do not change, but those of the nondispersive mirrors do. Moreover these results indicate that the presence of a dispersive material in the defect region causes the microcavity to perform badly in comparison with its nondispersive-material counterpart.

5. METAL/DIELECTRIC ONE-DIMENSIONAL PHOTONIC BANDGAP STRUCTURES

To push the limits of the dispersive characteristics of the PBG materials, we considered metals at optical frequencies. It has been discussed previously¹¹ that metals are modeled appropriately with dispersive-material models at these frequencies. We considered aluminum and gold as the dispersive metals in our studies; these materials were selected because they could lead to realizable PBG structures. The refractive indices of these metals at the wavelength 780 nm ($\omega_C = 2.417 \times 10^{15}$) and their corresponding Lorentz material-model parameters are listed in Table 2. It was assumed that $\omega_p = \omega_0$ and $\chi_L = 10$ for both materials. We specifically investigated PBG structures composed of layers of aluminum and dielectric or gold and dielectric, where the dielectric materials were taken to be nondispersive.

Figures 14(a) and 14(b) show the results for PBG structures consisting of a varying number of layers in the case of no defect. The basic shapes of these curves are very similar. Both structures can act as very highly reflective mirrors and conversely as bandpass filters at selected frequencies. However, the magnitude of the coefficients, the frequencies at which their peaks occur, and the sharpness of the rising or falling edges near the enhancement frequencies depend on the materials that compose the PBG structures. The resonance frequencies of the materials decide the locations where the transmission coefficients are nearly zero (reflection coefficients are nearly one), and the damping coefficients decide the degree of sharpness of the rising and falling edges of these curves. The PBG structures for use as highly reflective mirrors and narrow bandpass filters that are constructed of gold can outperform those composed of aluminum, as shown in Figs. 14(a) and 14(b).

The corresponding microcavity (PBG mirrors with air defect) results are shown in Figs. 15(a) and 15(b). The sources again are located in the centers of the defects. The peaks of the transmission coefficients in Fig. 15(a) are much larger for the smallest number of layers, i.e., for three layers and ω near $1.5\omega_C$. The widths of these peaks are much lower as the number of layers increases. Also, as the number of lossy, dispersive layers is in-

creased, less energy is coupled from the interior of the PBG microcavity to its exterior; i.e., the peaks of the transmission-coefficient curves decrease as the number of layers is increased. Nonetheless, these dispersive-mirror microcavity structures, particularly the gold-based ones, still exhibit large enhancements at specific frequencies even when a large number of layers are present. These opposing behaviors of the transmission peaks and their widths demonstrate that there are definitive trade-offs in the design of these metallic PBG microcavities.

Notice, however, that there are some large transmission-coefficient values in Fig. 15(b) even for the many-layer gold PBG microcavities in the high-frequency regions, e.g., between 1.3 and 1.5. The number of peaks in a transmission-coefficient curve in these passband re-

Table 2. Lorentz Material-Model Properties of Aluminum and Gold at 780 nm

Material	Refractive Index	ω_0	Γ
Al	$2.6 - j8.2$	$0.9492\omega_C$	$0.0686\omega_C$
Au	$0.175 - j4.91$	$0.8461\omega_C$	$0.0195\omega_C$

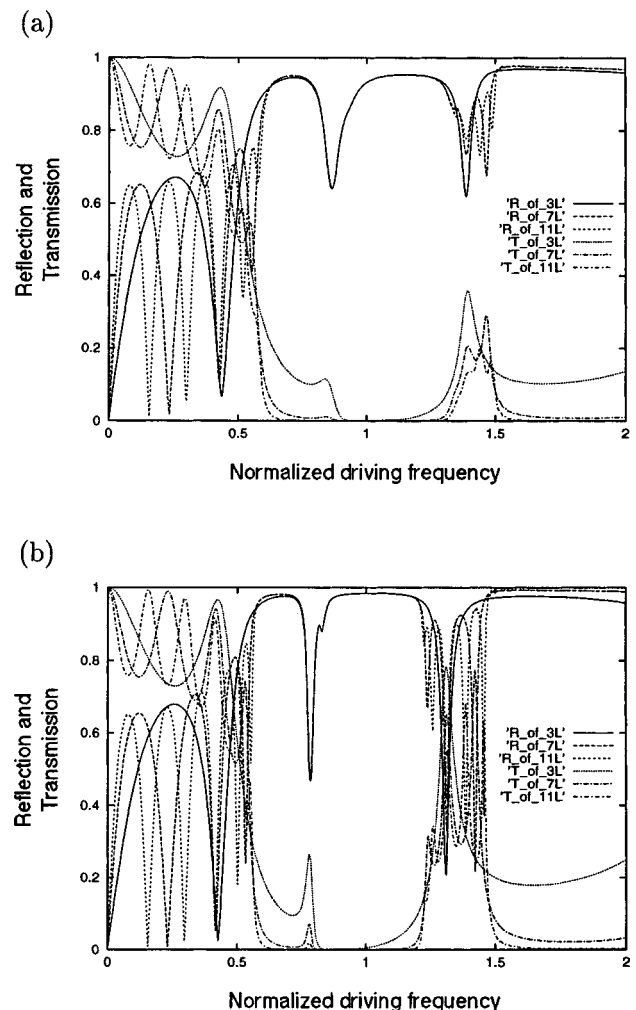


Fig. 14. Reflection and transmission coefficients versus normalized driving frequency for 3-, 7-, and 11-layer-mirror PBG structures. The PBG is composed of (a) aluminum and dielectric layers and (b) gold and dielectric layers.

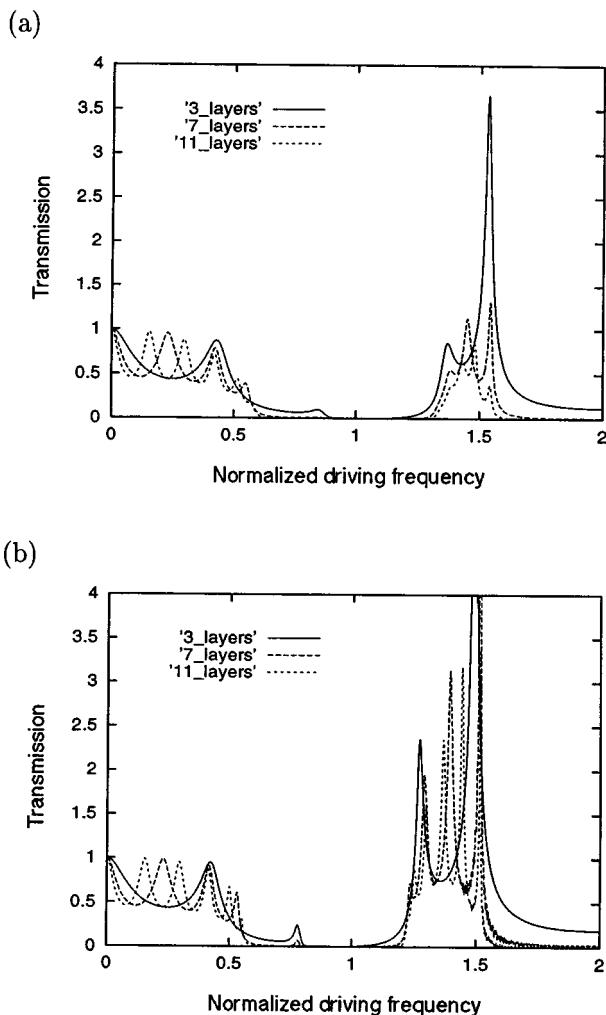


Fig. 15. Transmission coefficient versus normalized driving frequency for an n -layer-mirror PBG microcavity with an air defect. The PBG mirrors are composed of (a) aluminum and dielectric layers and (b) gold and dielectric layers.

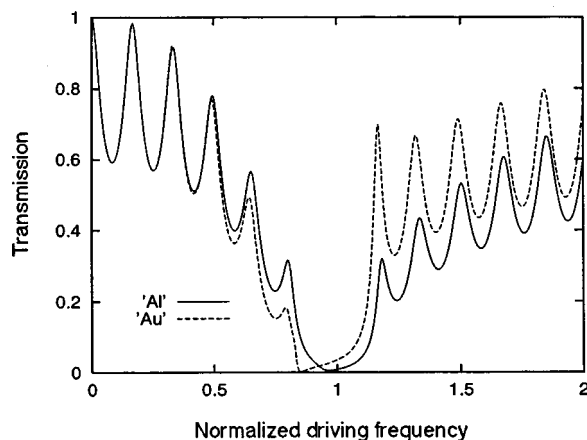


Fig. 16. Transmission coefficient versus normalized driving frequency for a PBG microcavity formed by an aluminum or a gold defect sandwiched between a pair of 11-layer nondispersive mirrors.

gions depends on the number of layers in the PBG mirrors. Multiple peaks occur for a larger number of layers. This means that these source-driven dispersive-mirror microcavity structures could be designed to produce

multiple-frequency outputs. These source structures could have a variety of potential wavelength-division-multiplexing applications.

Finally, Fig. 16 indicates the corresponding results for the case in which the microcavities are composed of non-dispersive PBG mirrors with aluminum or gold defect regions. The resonance frequencies in media 1 and 2 are again $\omega_{01} = \omega_{02} = 100\omega_C$, and the material parameters listed in Table 2 are used for the defect region. The transmission coefficient for the gold defect is always larger than that of the aluminum defect for frequencies above the center frequency. This behavior is due simply to the fact that the aluminum defect is more lossy electromagnetically than the gold defect. Nonetheless, this case again demonstrates the advantages of the dispersive mirrors and the nondispersive-defect PBG structures.

6. CONCLUSIONS

Photonic bandgap (PBG) structures constructed from lossy, dispersive dielectric or metallic materials were characterized in terms of their reflection and transmission properties. These PBG structures were modeled analytically with an $ABCD$ matrix approach and numerically with a FDTD simulator combined with a FFT post-processor. PBG structures with and without defects were considered.

It was shown that material dispersion can significantly alter the electromagnetic responses of the PBG structures, particularly if the resonance frequency of the Lorentz model is near the center frequency of the bandgap. The locations and quality of the bandgaps and passbands are altered. Results were given to characterize some of these changes. It was also shown that microcavities whose mirrors are constructed from dispersive-mirror PBG structures can outperform similar nondispersive-mirror microcavities. Metal/dielectric PBG structures, which are highly dispersive at optical frequencies, were discussed. They were shown to exhibit transmission characteristics significantly different from those of their dielectric counterparts. For instance, despite the presence of metals with very shallow skin depths, these very lossy, dispersive-material structures were shown to have strong transmissive properties in certain frequency regimes. It was also shown that large enhancements at specific frequencies could be obtained for the corresponding source-driven dispersive-mirror-microcavity PBG structures.

These results for lossy, dispersive-material PBG structures are currently being extended to higher dimensions for both scattering and guided-wave applications. The results of these studies will be reported elsewhere in the near future.

ACKNOWLEDGMENTS

This work was sponsored in part by the U.S. Office of Naval Research under grant N0014-95-1-0636 and by the U.S. Air Force Office of Scientific Research, Air Force Materiel Command, USAF, under grant F49620-96-1-0039.

REFERENCES

1. V. Radisic, Y. Qian, and T. Itoh, "Broad-band power amplifier using dielectric photonic bandgap structure," *IEEE Microwave Guided Wave Lett.* **8**, 13–15 (1998).
2. V. Radisic, Y. Qian, R. Coccioli, and T. Itoh, "Novel 2-D photonic bandgap structure for microstrip lines," *IEEE Microwave Guided Wave Lett.* **8**, 69–71 (1998).
3. E. Yablanovich, "Inhibited spontaneous emission in solid-state physics and electronics," *Phys. Rev. Lett.* **58**, 2059–2062 (1987).
4. D. Maystre, "Electromagnetic study of photonic band gaps," *Pure Appl. Opt.* **3**, 975–993 (1994).
5. J. D. Joannopoulos, R. D. Meade, and J. N. Winn, *Photonics Crystals: Molding the Flow of Light* (Princeton U. Press, Princeton, N.J., 1995).
6. R. W. Ziolkowski, "FDTD Modeling of photonic nanometer-sized power splitters and switches," in *Integrated Photonics Research*, Vol. 4 of 1998 OSA Technical Digest Series (Optical Society of America, Washington, D.C., 1998), pp. 175–177.
7. S. Kawakami, "Fabrication processes for 3D periodic nanostructures and photonic crystals," in *Integrated Photonics Research*, Vol. 4 of 1998 OSA Technical Digest Series (Optical Society of America, Washington, D.C., 1998), pp. 178–180.
8. B. D'Urso, O. Painter, A. Yariv, and A. Scherer, "Membrane microresonator lasers with 2-D photonic bandgap crystal mirrors for compact in-plane optics," in *Integrated Photonics Research*, Vol. 4 of 1998 OSA Technical Digest Series (Optical Society of America, Washington, D.C., 1998), pp. 181–183.
9. O. Painter, R. Lee, A. Yariv, and A. Scherer, "Photonic bandgap membrane microresonator," in *Integrated Photonics Research*, Vol. 4 of OSA Technical Digest Series (Optical Society of America, Washington, D.C., 1998), pp. 221–223.
10. J. A. Kong, *Electromagnetic Wave Theory* (Wiley, New York, 1986), pp. 120–132.
11. J. B. Judkins and R. W. Ziolkowski, "Finite-difference time-domain modeling of nonperfectly conducting metallic thin-film gratings," *J. Opt. Soc. Am. A* **12**, 1974–1983 (1995).
12. M. J. Bloemr and M. Scalora, "Transmissive properties of Ag/MgF₂ photonic band gaps," *Appl. Phys. Lett.* **72**, 1676–1678 (1998).
13. A. Taflove, *Computational Electrodynamics* (Artech House, Boston, Mass., 1995), pp. 111–134.